

# Pano3DComposer: Feed-Forward Compositional 3D Scene Generation from Single Panoramic Image

Zidian Qiu    Ancong Wu\*

Sun Yat-sen University

qiuzd@mail2.sysu.edu.cn, wuanc@mail.sysu.edu.cn

## Abstract

Current compositional image-to-3D scene generation approaches construct 3D scenes by time-consuming iterative layout optimization or inflexible joint object-layout generation. Moreover, most methods rely on limited field-of-view perspective images, hindering the creation of complete 360° environments. To address these limitations, we design **Pano3DComposer**, an efficient feed-forward framework for panoramic images. To decouple object generation from layout estimation, we propose a plug-and-play **Object-World Transformation Predictor**. This module converts the 3D objects generated by off-the-shelf image-to-3D models from local to world coordinates. To achieve this, we adapt the VGGT architecture to **Alignment-VGGT** by using target object crop, multi-view object renderings and camera parameters to predict the transformation. The predictor is trained using pseudo-geometric supervision to address the shape discrepancy between generated and ground-truth objects. For input images from unseen domains, we further introduce a **Coarse-to-Fine (C2F) alignment mechanism** for Pano3DComposer that iteratively refines geometric consistency with feedback of scene rendering. Our method achieves superior geometric accuracy for image/text-to-3D tasks on synthetic and real-world datasets. It can generate a high-fidelity 3D scene in approximately 20 seconds on an RTX 4090 GPU. The project page is available [here](#).

## 1. Introduction

High-quality 3D scene generation underpins applications in VR/AR and digital twins. Despite rapid advances in 3D generation, handling complex multi-object scenes from a single image remains challenging. Currently, most advanced image-to-3D pipelines rely on perspective images, which suffer from a limited field-of-view. Conversely, panoramic images overcome this restriction by offering rich spatial context of the entire environment, enabling the gen-

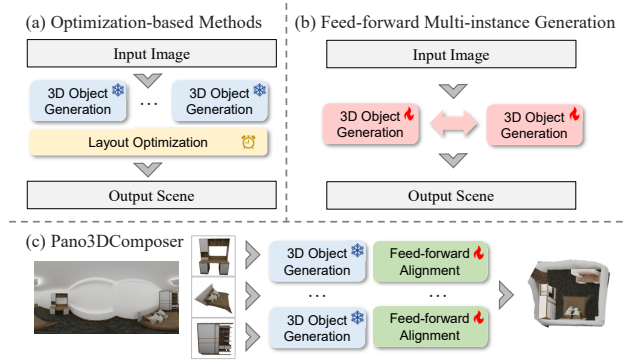


Figure 1. Paradigms of compositional 3D scene generation.

eration of geometrically complete 360° 3D scenes.

Existing 3D scene generation methods primarily fall into the following categories. Feed-forward scene understanding methods [3, 23, 28, 45] jointly predict layout, object geometry and poses using encoder-decoder architectures, which are efficient for inference but limited by lack of precise 3D mesh supervision and out-of-distribution generalization. Feed-forward multi-instance generative models [14, 27] extend single-object generators to jointly synthesize multiple instances and the layouts, often requiring costly fine-tuning. Compositional optimization-based pipelines [1, 4, 9, 13, 19, 41, 49, 50] separate asset generation from pose/layout optimization. Unfortunately, these methods usually rely on time-consuming iterative optimization processes, making it difficult to meet efficiency requirements. The above discussed methods trained on perspective images are not directly applicable to equirectangular panoramas, because panoramic images exhibit severe distortion, non-uniform sampling, and view-dependent distance/angle foreshortening. Only a few approaches [5, 44] focus on addressing panoramic images, but these methods are limited to generating meshes without textures that cannot compose a render-ready 3D scene.

To overcome the limitation of time-consuming optimization and inflexible joint object-layout generation of exist-

\*Corresponding author: wuanc@mail.sysu.edu.cn

ing methods, we design Pano3DComposer, a modular feed-forward framework for compositional 3D scene generation from a single panorama, as shown in Figure 1. The core modules of the framework are the 3D Object Generator and the Object-World Transformation Predictor, which decouple object generation from layout estimation.

For object generation, we first segment and project each instance crop from the panorama into the perspective domain, mitigating panoramic distortion. An off-the-shelf 3D Object Generator then produces high-quality meshes or 3D Gaussian splats [16] from this localized input.

To position the generated object in the scene, we formulate the object-to-world transformation as a cross-coordinate geometric mapping problem. The Object-World Transformation Predictor learns the conversion from object renderings of the generated object to the cropped input. To achieve this, we adapt the VGGT [37] architecture to Alignment-VGGT, which takes multi-view object renderings, target object crop and their corresponding camera parameters as input to estimate object-to-world rotation, translation, and anisotropic scale in a single feed-forward pass. Furthermore, to handle shape discrepancies between generated and ground-truth (GT) objects, the transformation predictor is trained using pseudo-geometry supervision distilled from differentiable optimizers, instead of GT mesh supervision.

To handle inputs from unseen domains, we further introduce the Coarse-to-Fine (C2F) alignment mechanism that iteratively refines the geometric consistency of each object using feedback from the current scene rendering.

The feed-forward nature of our framework ensures efficient inference, while its modular design guarantees flexibility that components can be trained independently, and off-the-shelf 3D object generator can be integrated without training. Our contributions are summarized as follows:

- A plug-and-play Object-World Transformation Predictor module based on the Alignment-VGGT architecture enables efficient alignment of a generated 3D object with the target panoramic scene rendering in a forward pass.
- A coarse-to-fine alignment mechanism that progressively improves object-to-scene alignment without gradient-based optimization.
- Extensive experiments on synthetic and real scenes demonstrate superior geometric accuracy and inference efficiency compared to state-of-the-art methods.

## 2. Related Work

### 2.1. Text/Image-to-3D Object Generation

Diffusion-driven 3D generation has advanced rapidly. For text-to-3D, DreamFusion [30] introduced Score Distillation Sampling (SDS), enabling 3D synthesis from 2D diffusion models [11]. Follow-ups [22] adopt more efficient 3D rep-

resentations such as 3D Gaussian Splatting (3DGS) [16] to improve quality and efficiency. Recent work further leverages text-to-point-cloud initialization and human priors [21, 43], or structured noise for variational 3DGS [20]. For image-to-3D, methods adapt 2D diffusion models for multi-view synthesis [24, 26, 32, 33] and accelerate single-view reconstruction with feed-forward networks such as LRM [12] and LGM [36]. Asset-level training on 3D models further boosts geometric fidelity, as demonstrated by CLAY [46] and TRELLIS [40]. However, these approaches primarily focus on single objects and remain limited in multi-object composition. In contrast, we extend single-object generators to compositional scene synthesis via a plug-and-play transformation predictor that aligns multiple objects within 360° panoramic views.

### 2.2. 3D Scene Generation

**Feed-forward 3D scene generation.** Early methods such as Total3D [28] jointly estimate layout, object poses, and shapes from a single image; follow-ups including Im3D [45] and InstPIFu [23] adopt implicit representations for indoor reconstruction, or apply 3D diffusion conditioned on input images [3]. Extensions to panoramas such as DeepPanoContext [44] and PanoContext-Former [5] recover room layouts and object geometry from a single panoramic image. Another line of research extends large single-object generators to multi-object generation, including MIDI [14] and SceneGen [27]. CAST [42] directly predict alignment parameters in a single forward pass. However, these approaches suffer from tight coupling between the object generation module and the alignment module, making it difficult to adopt a plug-and-play design that would allow flexible switching among different object generation models. They also suffer from high training costs and limited handling of panoramic distortions. Unlike these methods, our approach decouples object generation from spatial alignment, enabling flexible integration of any 3D object generator while efficiently handling panoramic distortions through perspective projection.

**Compositional 3D scene generation.** Compositional pipelines decouple object generation and layout optimization, often aided by LLMs for layout planning, exemplified by GALA3D [50] and LayoutYour3D [49]. Several approaches optimize object poses via differentiable rendering or depth alignment, including REPARO [10] and Gen3DSR [1], while others retrieve and compose objects from 3D databases, e.g., Holodeck [41]. Recent efforts, represented by HiScene [4] and ArtiScene [9], advance amodal completion and object generation quality. However, they are significantly affected by occlusions in RGB input and inaccuracies in estimated depth, which interfere with pose optimization and prevent precise alignment with the input image. Moreover, most pipelines either rely on slow iterative

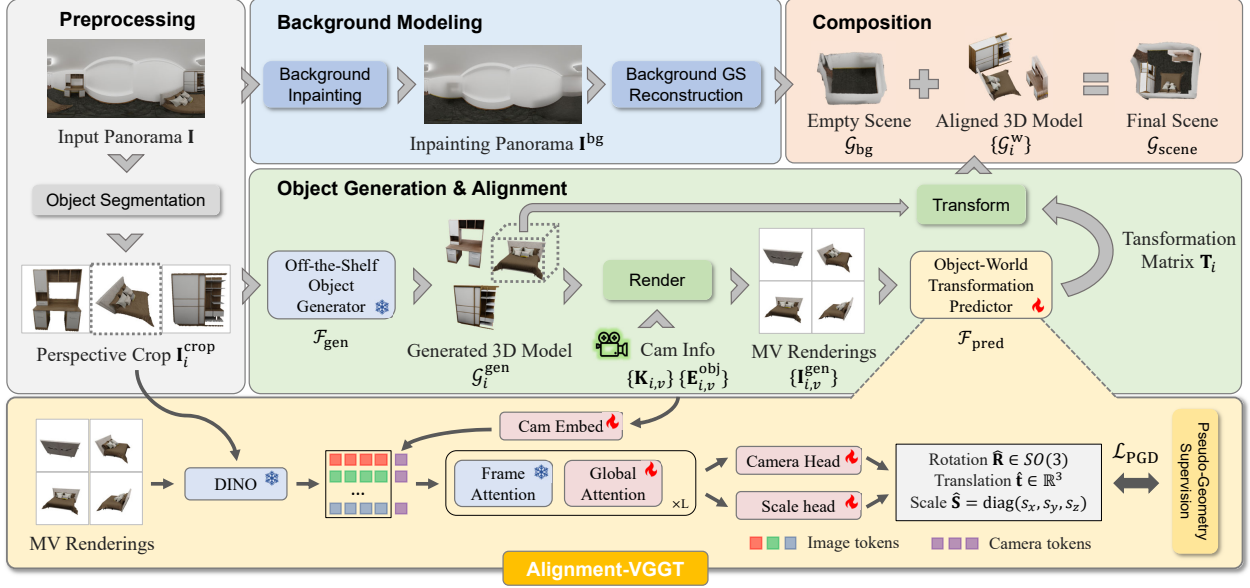


Figure 2. **Overview of Pano3DComposer.** The framework takes a panoramic image  $\mathbf{I}$  as input and generates a 3D scene  $\mathcal{G}_{\text{scene}}$  through four stages: (i) Preprocessing, (ii) Object Generation & Alignment, (iii) Background Modeling, and (iv) Composition.

optimization, and failing to address the unique challenges of panoramic inputs. Our method overcomes these limitations by a feed-forward transformation predictor trained with pseudo-geometry supervision, achieving efficient alignment specifically for panoramas.

### 3. Pano3DComposer

In this section, we introduce Pano3DComposer, a feed-forward modular framework for fast generation of geometrically complete 360° environments from panoramic images.

#### 3.1. Overall Framework

Given an equirectangular panorama  $\mathbf{I} \in \mathbb{R}^{H \times W \times 3}$ , we aim to reconstruct a compositional 3D scene consisting of a set of objects  $\{\mathcal{G}_i^w\}_{i=1}^N$  and background  $\mathcal{G}_{\text{bg}}$  in the world coordinate system. The overall rendering of  $\{\mathcal{G}_i^w\} \cup \mathcal{G}_{\text{bg}}$  should be consistent with  $\mathbf{I}$  both photometrically and geometrically.

Our framework consists of four stages: (i) Preprocessing, (ii) Object Generation and Alignment, (iii) Background Modeling, and (iv) Composition, as shown in Figure 2. First, the preprocessing module takes the panoramic image  $\mathbf{I}$  as input and outputs a set of distortion-free perspective crops  $\{\mathbf{I}_i^{\text{crop}}\}_{i=1}^N$  for each detected object. Then, each crop is fed into the 3D object generator  $\mathcal{F}_{\text{gen}}$  to produce 3D object asset  $\mathcal{G}_i^{\text{gen}}$  represented in the object’s local coordinate system. The core module Object-World Transformation Predictor  $\mathcal{F}_{\text{pred}}$  learns to predict the coordinate transformation  $\mathbf{T}_i = \mathcal{F}_{\text{pred}}(\mathbf{I}_i^{\text{crop}}, \mathcal{G}_i^{\text{gen}})$ . The transformation  $\mathbf{T}_i$  converts asset  $\mathcal{G}_i^{\text{gen}}$  from local to world coordinate system, in order to obtain  $\mathcal{G}_i^w = \{\mathbf{T}_i \mathbf{p} \mid \mathbf{p} \in \mathcal{G}_i^{\text{gen}}\}$  that is aligned

with the input panorama. The background modeling module reconstructs a 3D scene representation  $\mathcal{G}_{\text{bg}}$  from the inpainted image  $\mathbf{I}^{\text{bg}}$ . Finally, the composition module fuses  $\mathcal{G}_i^w$  and  $\mathcal{G}_{\text{bg}}$  to obtain a geometrically complete 3D scene.

#### 3.2. Object Generation and Alignment

##### 3.2.1. 3D Object Generator

**Preprocessing.** Given an equirectangular panoramic image  $\mathbf{I} \in \mathbb{R}^{H \times W \times 3}$  that encodes a full 360° view of the scene, each pixel corresponds to a direction defined by longitude and latitude angles  $(\theta, \phi)$ . We first apply open-vocabulary 2D foundation models on the panoramic image, e.g., SAM [17], to extract masks  $\{\mathbf{M}_i\}_{i=1}^N$  for each object. Let  $\Pi_{\text{persp}}(\cdot; \theta, \phi, \alpha)$  denote a perspective projection operator parameterized by longitude  $\theta \in [-\pi, \pi)$ , latitude  $\phi \in [-\frac{\pi}{2}, \frac{\pi}{2}]$ , and field-of-view  $\alpha \in (0, \pi)$ . For each object, we use its corresponding  $(\theta_i, \phi_i, \alpha_i)$  to transform the masked object from panorama coordinates to the distortion-free perspective crops  $\{\mathbf{I}_i^{\text{crop}}\}_{i=1}^N$  by

$$\mathbf{I}_i^{\text{crop}} = \Pi_{\text{persp}}(\mathbf{I} \odot \mathbf{M}_i; \theta_i, \phi_i, \alpha_i). \quad (1)$$

**3D object generation.** With the distortion-free perspective crops  $\mathbf{I}_i^{\text{crop}}$ , any off-the-shelf image-to-3D method can be employed to reconstruct the object as a mesh or a set of Gaussian splats. We denote the generated object by  $\mathcal{G}_i^{\text{gen}}$ , of which the 3D point set of  $\mathcal{G}_i^{\text{gen}}$  is denoted by  $\mathcal{P}_i^{\text{gen}} = \{(x_j^{\text{obj}}, y_j^{\text{obj}}, z_j^{\text{obj}})\}_{j=1}^M$  in the local coordinate system.

We use TRELLIS [40] as the default generator due to its high-fidelity geometry on mildly occluded instances; for

severe occlusion we optionally adopt amodal completion (e.g., Amodal3R [39]) to improve geometric completeness.

### 3.2.2. Object-World Transformation Predictor

**Cross-coordinate geometric mapping problem.** The core challenge is accurately placing each generated object  $\mathcal{G}_i^{\text{gen}}$  by estimating the transformation  $\mathbf{T}_i$  (rotation, translation, scale) to convert the object from its local coordinates to world coordinates for alignment with panorama  $\mathbf{I}$ .

A straightforward approach is to perform 3D alignment between the generated object and the scene geometry estimated from the monocular panorama. However, accurately reconstructing 3D geometry from a single panoramic image is still very difficult, leading to alignment errors. To avoid this limitation, we shift the task from the challenging 3D space to more robust 2D image space. We represent the 3D asset using multi-view renderings that captures geometry and texture details, and then seek correspondence with the target perspective object crop from the panorama.

**Preliminaries of VGGT.** Recently, visual-geometry foundation models [15, 37] have achieved remarkable success. These models, such as Visual Geometry Grounded Transformer (VGGT) [37], take multi-view RGB images as input and predict a set of 3D attributes in a forward pass, including camera parameters, depth maps, and point clouds.

Current foundation models are typically restricted to processing multi-view inputs captured from the same 3D scene that share the same coordinate system and camera parameters. However, the cross-coordinate geometric mapping problem involves input images captured by different camera parameters and represented in different coordinate systems. **Alignment-VGGT.** To construct the Object-World Transformation Predictor  $\mathcal{F}_{\text{pred}}$ , we introduce Alignment-VGGT, an adaptation of the VGGT architecture with specialized input structure and output heads to bridge this coordinate gap.

To represent the geometric and textural information of the generated object  $\mathcal{G}_i^{\text{gen}}$  in 2D space, we render multi-view images from  $V$  predefined viewpoints:

$$\{\mathbf{I}_{i,v}^{\text{gen}}\}_{v=1}^V = \Pi_{\text{render}}(\mathcal{G}_i^{\text{gen}}; \{\mathbf{K}_v, \mathbf{E}_v^{\text{obj}}\}_{v=1}^V), \quad (2)$$

where  $\mathbf{K}_v \in \mathbb{R}^{3 \times 3}$  and  $\mathbf{E}_v^{\text{obj}} = [\mathbf{R}_v^{\text{obj}} \mid \mathbf{t}_v^{\text{obj}}]$  denote the intrinsic matrix and extrinsic parameters for the  $v$ -th view.

As for the input structure, the vanilla VGGT model designates the first input image in the sequence as the reference frame for reconstruction. To adapt to this mechanism, we regard the perspective crop  $\mathbf{I}_i^{\text{crop}}$  as the target image for alignment and set it as the first input image. Then, we concatenate it with multi-view renderings  $\{\mathbf{I}_{i,v}^{\text{gen}}\}_{v=1}^V$  as input to Alignment-VGGT. Moreover, we also provide known camera parameters to avoid the intrinsic–extrinsic ambiguity when jointly estimating both parameters from images alone. Specifically, for each view (target crop or a multi-view rendered image), we encode its intrinsic matrix  $\mathbf{K} \in \mathbb{R}^{3 \times 3}$  and

extrinsic parameters  $\mathbf{E} = [\mathbf{R} \mid \mathbf{t}]$  via two separate linear projection layers, and then add this camera embedding to the corresponding camera token for that view as input to the transformer layers. This design explicitly disentangles camera geometry from visual features, enabling Alignment-VGGT to accurately resolve the cross-coordinate mapping even when intrinsics and scales differ between the local object frame and the world panorama frame.

Regarding the output head, the camera head in vanilla VGGT predicts the rotation and translation components of the extrinsics, omitting the scale transformation. We resolve this by augmenting Alignment-VGGT with a scale head, enabling the model to output a complete set of camera extrinsics for the local coordinates and the anisotropic scale factors for mapping to world coordinates.

The forward pass of Alignment-VGGT is formulated as:

$$\{\hat{\mathcal{E}}, \hat{\mathbf{S}}\} = \mathcal{F}_{\text{a-vgggt}}(\mathbf{I}_i^{\text{crop}}, \{\mathbf{I}_{i,v}^{\text{gen}}\}_{v=1}^V, \{\mathbf{K}_v\}_{v=0}^V, \{\mathbf{E}_v^{\text{obj}}\}_{v=1}^V). \quad (3)$$

The network inputs include (i) the target crop  $\mathbf{I}_i^{\text{crop}}$  and its intrinsics  $\mathbf{K}_0$ , (ii) multi-view renderings  $\{\mathbf{I}_{i,v}^{\text{gen}}\}_{v=1}^V$  with their known intrinsics  $\{\mathbf{K}_v\}_{v=1}^V$  and extrinsics  $\{\mathbf{E}_v^{\text{obj}}\}_{v=1}^V$  in the local frame. Note that  $\mathbf{E}_0^{\text{obj}}$  is unknown and not provided as input. The network outputs predicted poses for all views and anisotropic scale:

$$\hat{\mathcal{E}} = \left\{ \hat{\mathbf{E}}_v = [\hat{\mathbf{R}}_v^{\text{obj}} \mid \hat{\mathbf{t}}_v^{\text{obj}}] \right\}_{v=0}^V, \hat{\mathbf{S}} = \text{diag}(\hat{s}_x, \hat{s}_y, \hat{s}_z), \quad (4)$$

which are defined in Aignment-VGGT coordinate system.

Then, we infer the unknown local extrinsics by relative pose chaining. First, we compute the coordinate-invariant relative transformation from view 1 to view 0 in the Aignment-VGGT coordinate system, and then apply it to the known extrinsics in the object’s local coordinate system:

$$\mathbf{E}_0^{\text{obj}} = \Delta \mathbf{E}_{1 \rightarrow 0} \mathbf{E}_1^{\text{obj}}, \quad (5)$$

where  $\Delta \mathbf{E}_{1 \rightarrow 0} = \hat{\mathbf{E}}_0 \hat{\mathbf{E}}_1^{-1}$ .

Given  $\mathbf{E}_0^{\text{obj}}$  in the local frame and  $\mathbf{E}_i^{\text{crop}} = [\mathbf{R}_i^{\text{w}} \mid \mathbf{t}_i^{\text{w}}]$  in the world frame, we compose the non-rigid transformation incorporating the predicted anisotropic scale:

$$\mathbf{T}_i = \begin{bmatrix} \mathbf{R}_i^{\text{w}} & \mathbf{t}_i^{\text{w}} \\ \mathbf{0}^\top & 1 \end{bmatrix} \begin{bmatrix} (\mathbf{R}_0^{\text{obj}})^\top & -(\mathbf{R}_0^{\text{obj}})^\top \mathbf{t}_0^{\text{obj}} \\ \mathbf{0}^\top & 1 \end{bmatrix} \begin{bmatrix} \hat{\mathbf{S}} & \mathbf{0} \\ \mathbf{0}^\top & 1 \end{bmatrix}. \quad (6)$$

Finally, we apply the transformation  $\mathbf{T}_i$  to convert the generated object from the local coordinate system to the world coordinate system:

$$\mathcal{G}_i^{\text{w}} = \{\mathbf{T}_i \mathbf{p} \mid \mathbf{p} \in \mathcal{G}_i^{\text{gen}}\}, \quad (7)$$

where each point  $\mathbf{p} = [x^{\text{obj}}, y^{\text{obj}}, z^{\text{obj}}, 1]^\top$  belongs to the 3D point set  $\mathcal{P}_i^{\text{gen}}$  of  $\mathcal{G}_i^{\text{gen}}$ . For mesh representations, we

simply transform vertex positions. For 3D Gaussian Splatting representations, in addition to transforming Gaussian centers, we also transform their covariance matrices by applying the rotation and scale components of  $\mathbf{T}_i$  to ensure proper orientation and shape in the world frame.

### 3.2.3. Loss Functions

After obtaining the transformed object  $\mathcal{G}_i^w$  via the predicted transformation, a key challenge arises in training the predictor: directly supervising with ground-truth (GT) mesh poses is infeasible due to inevitable shape discrepancies between the generated object  $\mathcal{G}_i^{\text{gen}}$  and the GT mesh  $\mathcal{G}_i^{\text{GT}}$ . Even if GT pose annotations were available, they would correspond to the GT geometry rather than the generated geometry, leading to misaligned supervision signals.

To address this issue, we adopt a pseudo-geometry supervision scheme that distills transformation parameters from slow but reliable offline optimizers. For each generated object, we run an offline differentiable optimization to fit rotation  $\mathbf{R} \in \text{SO}(3)$ , translation  $\mathbf{t} \in \mathbb{R}^3$ , and anisotropic scale  $\mathbf{S} = \text{diag}(s_x, s_y, s_z)$ . The resulting parameters  $(\mathbf{R}^*, \mathbf{t}^*, \mathbf{S}^*)$  define a transformation from the generated object to its GT mesh.

**Supervision with GT meshes.** When GT 3D meshes are available, we optimize the transform using a bidirectional Chamfer loss. Let  $\mathcal{P}^w$  denote the set of points sampled from the generated object transformed from the  $i$ -th object, and  $\mathcal{P}$  be points from the GT mesh. We define:

$$\mathcal{L}_{\text{CD}}^{\text{bi}}(\mathcal{P}^w, \mathcal{P}) = \frac{1}{|\mathcal{P}^w|} \sum_{\hat{\mathbf{p}} \in \mathcal{P}^w} \min_{\mathbf{p} \in \mathcal{P}} \|\hat{\mathbf{p}} - \mathbf{p}\|_2^2 + \frac{1}{|\mathcal{P}|} \sum_{\mathbf{p} \in \mathcal{P}} \min_{\hat{\mathbf{p}} \in \mathcal{P}^w} \|\mathbf{p} - \hat{\mathbf{p}}\|_2^2, \quad (8)$$

the offline optimization minimizes:

$$(\mathbf{R}^*, \mathbf{t}^*, \mathbf{S}^*) = \arg \min_{\mathbf{R}, \mathbf{t}, \mathbf{S}} \mathcal{L}_{\text{CD}}^{\text{bi}}(\mathcal{P}^w, \mathcal{P}). \quad (9)$$

**Supervision with monocular RGBD.** When GT meshes are unavailable, we back-project GT depth into a partial point cloud  $\mathcal{P}$  and use a single-directional Chamfer loss:

$$\mathcal{L}_{\text{CD}}^{\text{si}}(\mathcal{P}^w, \mathcal{P}) = \frac{1}{|\mathcal{P}|} \sum_{\mathbf{p} \in \mathcal{P}} \min_{\hat{\mathbf{p}} \in \mathcal{P}^w} \|\mathbf{p} - \hat{\mathbf{p}}\|_2^2. \quad (10)$$

To mitigate inaccuracies from asymmetric point-to-surface matching, we augment  $\mathcal{L}_{\text{CD}}^{\text{si}}$  with a mask loss

$$\mathcal{L}_{\text{MASK}} = \|\mathbf{M} - \hat{\mathbf{M}}\|_2^2 + 1 - \text{IoU}(\mathbf{M}, \hat{\mathbf{M}}), \quad (11)$$

where  $\hat{\mathbf{M}}$  denotes the rendered mask and  $\mathbf{M}$  denotes the instance mask. The optimization becomes:

$$(\mathbf{R}^*, \mathbf{t}^*, \mathbf{S}^*) = \arg \min_{\mathbf{R}, \mathbf{t}, \mathbf{S}} (\mathcal{L}_{\text{CD}}^{\text{si}}(\mathcal{P}^w, \mathcal{P}) + \lambda_{\text{MASK}} \mathcal{L}_{\text{MASK}}). \quad (12)$$

**Training objective.** During training of the Object-World Transformation Predictor, given transformation parameters

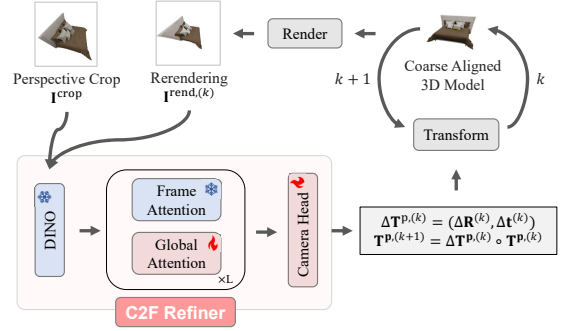


Figure 3. Illustration of the proposed Coarse-to-Fine (C2F) alignment mechanism.

$(\mathbf{R}^*, \mathbf{t}^*, \mathbf{S}^*)$  and predictions  $(\hat{\mathbf{R}}, \hat{\mathbf{t}}, \hat{\mathbf{S}})$ , we regress parameters with element-wise L1 losses. For rotation, we convert to unit quaternions and, after normalization and sign alignment, apply element-wise L1. Let  $\hat{\mathbf{q}} = \text{unit}(Q(\hat{\mathbf{R}}))$  and  $\mathbf{q}^* = \text{unit}(Q(\mathbf{R}^*))$ . The PGD loss is

$$\mathcal{L}_{\text{PGD}} = \|\hat{\mathbf{q}} - \mathbf{q}^*\|_1 + \|\hat{\mathbf{t}} - \mathbf{t}^*\|_1 + \|\text{diag}(\hat{\mathbf{S}}) - \text{diag}(\mathbf{S}^*)\|_1. \quad (13)$$

We also include the mask loss to enforce silhouette consistency between rendered mask of the transformed object and the input instance mask. The total training objective of Object-World Transformation Predictor is

$$\mathcal{L} = \lambda_{\text{CD}} \mathcal{L}_{\text{CD}} + \lambda_{\text{PGD}} \mathcal{L}_{\text{PGD}} + \lambda_{\text{MASK}} \mathcal{L}_{\text{MASK}}. \quad (14)$$

These serve as supervisory targets for the Object-World Transformation Predictor, replacing expensive per-instance optimization at inference with a single feed-forward pass.

### 3.3. Background Reconstruction and Scene Fusion

We merge all instance masks and apply an inpainting model (LaMa [34] or DiT360 [6]) on the panoramic image to obtain a clean background panorama  $\mathbf{I}^{\text{bg}}$ . A feed-forward Gaussian reconstruction network, following Flash3D [35], predicts background depth with Depth-Anywhere [38] and generates a background Gaussian set  $\mathcal{G}_{\text{bg}}$ . Finally, we place all aligned instances  $\{\mathcal{G}_i^w\}$  and fuse them with  $\mathcal{G}_{\text{bg}}$  in the world frame, producing the complete 3D scene  $\{\mathcal{G}_i^w\} \cup \mathcal{G}_{\text{bg}}$ .

## 4. Iterative Extension: Pano3DComposer-C2F

The initial placement produced by the Object-World Transformation Predictor may be imperfect when applied to unseen domains, due to distribution shift between training and testing data. To address this, we introduce a Coarse-to-Fine (C2F) alignment mechanism to extend Pano3DComposer to an iterative version called Pano3DComposer-C2F, which progressively refines the object position by more steps.

Compared with the Pano3DComposer, we additionally introduce a C2F Refiner module based on Alignment-VGGT with feedback of current rendering result. Given a

coarsely aligned object at pose  $\mathbf{T}^{\text{p},(k)} = (\mathbf{R}^{(k)}, \mathbf{t}^{(k)})$  where  $\mathbf{R}^{(k)} \in \text{SO}(3)$  and  $\mathbf{t}^{(k)} \in \mathbb{R}^3$ , we render it using the camera parameters of the perspective crop to obtain the current rendering  $\mathbf{I}^{\text{rend},(k)}$ . The refiner takes as input the concatenation of the current rendering  $\mathbf{I}^{\text{rend},(k)}$  and the target object crop  $\mathbf{I}^{\text{crop}}$  from the panorama, and estimates a relative pose update  $\Delta \mathbf{T}^{\text{p},(k)} = (\Delta \mathbf{R}^{(k)}, \Delta \mathbf{t}^{(k)})$  while keeping the scale fixed to avoid shape distortion:

$$\Delta \mathbf{T}^{\text{p},(k)} = \mathcal{F}_{\text{refine}}(\mathbf{I}^{\text{rend},(k)}, \mathbf{I}^{\text{crop}}). \quad (15)$$

The pose is then updated iteratively via composition:

$$\mathbf{T}^{\text{p},(k+1)} = \Delta \mathbf{T}^{\text{p},(k)} \circ \mathbf{T}^{\text{p},(k)}, \quad k = 0, 1, \dots, K_{\text{max}} - 1, \quad (16)$$

where  $\mathbf{T}^{\text{p},(0)}$  is the initial coarse pose from  $\mathcal{F}_{\text{pred}}$ .

During training, we supervise the refiner with the same pseudo-geometry distillation loss in Section 3.2.3. At inference time, we back-project depth estimated from the panorama into a point cloud  $\mathcal{P}_{\text{pseudo}}$  and monitor alignment quality via Chamfer distance  $\mathcal{L}_{\text{CD}}^{(k)}$  between the transformed object points and  $\mathcal{P}_{\text{pseudo}}$ . The iteration terminates when the improvement falls below a threshold  $\tau$  or the maximum iteration  $K_{\text{max}}$  is reached:

$$\mathcal{L}_{\text{CD}}^{(k)} - \mathcal{L}_{\text{CD}}^{(k+1)} < \tau \quad \text{or} \quad k + 1 = K_{\text{max}}. \quad (17)$$

This yields robust, feed-forward fine alignment without gradient-based optimization at test time, progressively correcting pose errors through rendering feedback.

## 5. Experiments

We conduct comprehensive experiments to validate the effectiveness of Pano3DComposer. Additional implementation details, qualitative results, visualizations, and ablation studies are provided in the supplementary material.

### 5.1. Experimental Setup

**Datasets.** We train and evaluate our model on two large-scale synthetic indoor datasets: 3D-FRONT [8] and Structured3D [48]. For 3D-FRONT, we render equirectangular panoramas and corresponding depth maps for each room using Blender, and utilize the ground-truth 3D meshes to generate pseudo-geometry supervision via bidirectional Chamfer distance optimization (Sec. 3.2.3). Since panoramas rendered from 3D-FRONT lack photorealism, we augment our training set with Structured3D, which provides photorealistic panoramas but only monocular depth without ground-truth meshes. For Structured3D, we employ single-directional Chamfer distance with mask regularization to derive pseudo-geometry supervision (Sec. 3.2.3). In total, we collect approximately 30,000 rooms, with 1,200 held out for testing. Additionally, we evaluate our method on a

collection of real-world panoramic images to assess generalization capability.

**Evaluation metric.** We evaluate the shape and layout accuracy using scene-level Chamfer Distance (CD-S) and F-Score (F-Score-S), object-level Chamfer Distance (CD-O) and F-Score (F-Score-O), and volumetric IoU of object bounding boxes (IoU-B).

**Compared methods for panorama-to-3D scene composition.** To comprehensively evaluate Pano3DComposer, which reconstructs a 3D scene from a single equirectangular panorama, we compare against DeepPanoContext [44], a method specifically designed for panoramic inputs, and SceneGen [27], a state-of-the-art feed-forward multi-instance generation method. Since SceneGen is designed exclusively for perspective images and cannot directly handle equirectangular panoramas due to distortion and non-uniform sampling, we fine-tune it on our panoramic 3D-FRONT dataset to enable a fair comparison with representative feed-forward approaches.

We also compare against two classical pose estimation baselines: Iterative Closest Point (ICP) [2] and differentiable optimization (OPT). For ICP, we use the implementation from the *small\_gicp* library [18] to align normalized point clouds extracted from the generated object and the reference image, followed by scaling with the estimated scale factor. For differentiable optimization, we optimize rotation, translation, and scale parameters to align the object with the reference RGB image and its corresponding depth prediction using a combination of photometric and geometric losses, as done in REPARO [10].

**Compared methods for text-to-3D scene generation.** We further evaluate Pano3DComposer in the Text-to-3D Scene Generation setting, where our pipeline first synthesizes a panoramic image from text using Diffusion360 [7], and subsequently composes the corresponding 3D scene conditioned on the generated panorama. For this task, we include representative text-to-3D scene methods GALA3D [50] and DreamScene [19].

### 5.2. Implementation Details

For the feed-forward Gaussian background model, we follow the pipeline of Flash3D [35], but replace its depth estimator with Depth-Anywhere [38] for improved monocular depth prediction on panoramas. For training the Object-World Transformation Predictor, we freeze the DINOv2 [29] backbone and frame attention layers of VGGT [37]. Mini-batch size is set as 1. Training on a single RTX 4090 takes roughly two days for both the Object-World Transformation Predictor and the C2F Refiner. The learning rate is set to  $1 \times 10^{-4}$  with a cosine decay schedule. Loss weights are set as  $\lambda_{\text{CD}} = 0.1$ ,  $\lambda_{\text{PGD}} = 1.0$ , and  $\lambda_{\text{MASK}} = 0.1$ . For the C2F refinement stage, we set the Chamfer distance threshold to  $\tau = 0.001$  and the maximum iteration

Table 1. Comparison of major and alignment results on the 3D-FRONT test set. The best performance for each metric is highlighted in **bold**. OPT represents differentiable optimization-based alignment, and ICP denotes Iterative Closest Point alignment. ‘‘Pseudo Geometry’’ serves as a reference upper bound obtained via offline differentiable optimization of the transformation parameters introduced in Sec. 3.2.3. Training resources are reported in 4090 GPU days. Inference time is tested on one 4090 GPU.

Method	CD-S↓	CD-O↓	F-Score-S↑	F-Score-O↑	IoU-B↑	Training Resources	Inference Time (s)
OPT	0.1059	0.1128	0.5535	0.5640	0.4010	–	120
ICP [18]	0.2483	0.2305	0.4524	0.4896	0.2830	–	<b>1</b>
DeepPanoContext [44]	0.7851	0.1657	0.3101	0.3822	0.0021	–	14
SceneGen [27]	0.1765	0.0914	0.4575	0.4827	0.1124	56 GPU days	63
Pano3DComposer (Ours)	0.0787	0.0765	0.6923	0.6926	0.5679	<b>2 GPU days</b>	20
Pano3DComposer-C2F (Ours)	<b>0.0784</b>	<b>0.0762</b>	<b>0.6930</b>	<b>0.6937</b>	<b>0.5699</b>	4 GPU days	24
<i>Pseudo Geometry</i>	0.0119	0.0119	0.8695	0.8781	0.8141	–	–

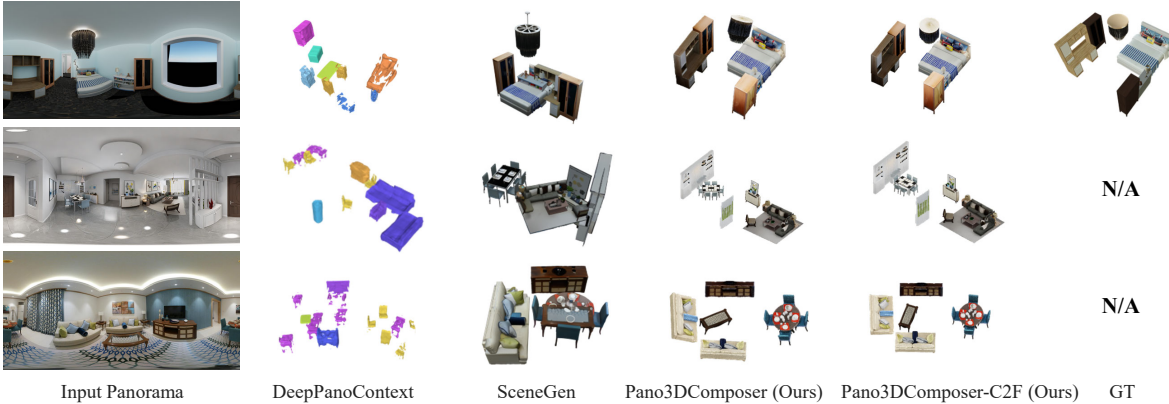


Figure 4. Visualization of panorama-to-3D scene composition results without background. Row 1: 3D-FRONT test set; Row 2: Structured3D test set; Row 3: real-world panoramas.

to  $K_{\max} = 5$ . For a fair comparison with the SceneGen baseline, we fine-tune from its released checkpoint on 3D-FRONT dataset using  $8 \times \text{RTX } 4090$  GPUs for 7 days to adapt it to equirectangular panoramic inputs.

### 5.3. Panorama-to-3D Scene Composition

Table 1 presents quantitative comparisons on the 3D-FRONT test set. Our Pano3DComposer achieves the best performance across all metrics while requiring significantly fewer training resources ( $1 \times 4090$ , 2d vs.  $8 \times 4090$ , 7d for SceneGen) and faster inference (20s vs. 63s per scene). Results in Table 1 also show that our predictor significantly outperforms both ICP and differentiable optimization. ICP struggles with outliers and symmetries, often converging to local minima. Differentiable optimization is sensitive to inaccurate depth estimates and occlusions, leading to suboptimal alignment. Our feed-forward predictor, trained with pseudo-geometry supervision, robustly estimates object poses from generated 3D models, achieving the best alignment performance.

Figure 4 shows qualitative comparisons in the panorama-to-3D task. DeepPanoContext fails to generate high-quality meshes due to limited supervised data. SceneGen struggles with panoramic distortion, resulting in incorrect spatial relationships. Our method mitigates distortion through

perspective projection and produces scenes with consistent geometry and plausible spatial relationships.

Pano3DComposer-C2F further improves alignment with marginal additional computational cost (24s vs. 20s). Beyond improvements on synthetic test set, the C2F mechanism also exhibits good generalization to real-world panoramas, as shown in Figure 5. As highlighted in the red boxes, C2F mechanism effectively corrects object positions through iterative refinement with rendering feedback. This validates the necessity and effectiveness of our iterative refinement mechanism for practical applications, enabling robust generalization to unseen data distributions without requiring expensive per-scene optimization. Table 2 provides a detailed breakdown of computational costs. These results demonstrate that our feed-forward transformation predictor and modular design enable accurate compositional 3D scene generation without sacrificing efficiency.

### 5.4. Text-to-3D Scene Generation

As shown in Figure 6, both GALA3D and DreamScene rely on Score Distillation Sampling (SDS) to optimize object appearance, which requires lengthy per-scene optimization (typically 30-60 minutes per object) and often leads to oversaturated colors and unrealistic textures. Moreover, these methods depend on LLM-generated layouts to deter-

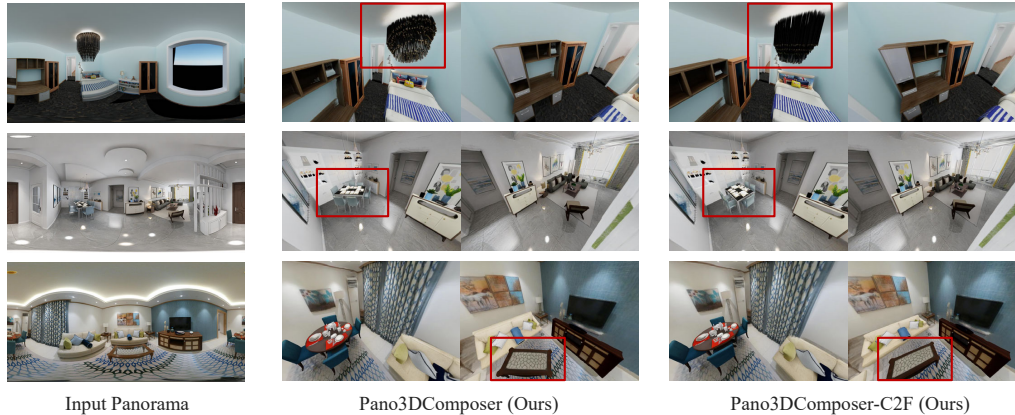


Figure 5. Visualization of panorama-to-3D scene composition results with background. The figure presents multi-view renderings of composed 3D scenes generated by our method. Row 1: 3D-FRONT test set; Row 2: Structured3D test set; Row 3: real-world panoramas.



Figure 6. Visualization of Text-to-3D scene generation results.

mine spatial arrangements, which frequently violate physical constraints and common spatial relationships. For instance, objects may float in mid-air, penetrate each other, or be placed at physically implausible positions.

In contrast, Pano3DComposer leverages state-of-the-art image-to-3D object generators to produce high-fidelity textured meshes, and derives spatial layouts directly from the synthesized panoramic image through our feed-forward transformation predictor. This design naturally respects the spatial context encoded in the panorama, ensuring physically plausible object arrangements. As a result, our method generates scenes with more realistic textures, accurate spatial relationships, and significantly improved efficiency.

### 5.5. Ablation Study

Table 3 compares the contributions of different losses and training strategies. Training with only the Chamfer loss  $\mathcal{L}_{CD}$  yields poor alignment quality, as the model fails to learn accurate pose regression without direct supervi-

Table 2. Runtime analysis of different processing stages.

Stage	Time (s)
Background Inpainting	0.02
Background GS Reconstruction	0.16
Object Generation (per object)	$\sim 4$
Object Alignment (per object)	0.36
Object Refinement (per step)	0.18

Table 3. Ablation study on loss functions and training strategies.

Method	CD-S $\downarrow$	CD-O $\downarrow$	F-Score-S $\uparrow$	F-Score-O $\uparrow$	IoU-B $\uparrow$
Only $\mathcal{L}_{CD}$	0.8688	0.9027	0.1980	0.1888	0.0906
+ $\mathcal{L}_{PGD}$	0.1266	0.1219	0.5675	0.5670	0.4670
+ $\mathcal{L}_{MASK}$	<b>0.1120</b>	<b>0.1063</b>	<b>0.5788</b>	<b>0.5850</b>	<b>0.4818</b>
w/o Cam info	0.1850	0.1705	0.4673	0.4691	0.3830

sion on transformation parameters, introducing the pseudo-geometry distillation loss  $\mathcal{L}_{PGD}$  substantially improves all metrics. Further adding the mask regularization  $\mathcal{L}_{MASK}$  brings additional gains, indicating that silhouette consistency is essential for spatial coherence. Excluding known camera intrinsics and extrinsics as input leads to a noticeable performance drop, further validating the importance of incorporating camera priors.

## 6. Conclusion

We presented Pano3DComposer, an efficient framework for compositional 3D scene generation from a single panorama. By learning a feed-forward Object-World Transformation Predictor with pseudo-geometry supervision, and applying a C2F alignment mechanism, our approach outperforms state-of-the-art methods across all metrics on 3D-FRONT dataset, and generalizes robustly to real-world panoramas through the C2F refinement mechanism. Our method generates high-fidelity 3D scenes in approximately 20 seconds per scene, making it practical for real-time applications in VR/AR and digital content creation.

## References

- [1] Andreea Ardelean, Mert Özer, and Bernhard Egger. Gen3dsr: Generalizable 3d scene reconstruction via divide and conquer from a single view. In *3DV*, 2025. 1, 2
- [2] Paul J Besl and Neil D McKay. Method for registration of 3-d shapes. *TPAMI*, 1992. 6
- [3] Manuel Dahnert, Angela Dai, Norman Müller, and Matthias Nießner. Coherent 3d scene diffusion from a single rgb image. *NIPS*, 2024. 1, 2
- [4] Wenqi Dong, Bangbang Yang, Zesong Yang, Yuan Li, Tao Hu, Hujun Bao, Yuwen Ma, and Zhaopeng Cui. Hiscene: creating hierarchical 3d scenes with isometric view generation. *arXiv*, 2025. 1, 2
- [5] Yuan Dong, Chuan Fang, Liefeng Bo, Zilong Dong, and Ping Tan. Panocontext-former: Panoramic total scene understanding with a transformer. In *CVPR*, 2024. 1, 2
- [6] Haoran Feng, Dizhe Zhang, Xiangtai Li, Bo Du, and Lu Qi. Dit360: High-fidelity panoramic image generation via hybrid training. *arXiv*, 2025. 5
- [7] Mengyang Feng, Jinlin Liu, Miaomiao Cui, and Xuansong Xie. Diffusion360: Seamless 360 degree panoramic image generation based on diffusion models. *arXiv*, 2023. 6
- [8] Huan Fu, Bowen Cai, Lin Gao, Ling-Xiao Zhang, Jiaming Wang, Cao Li, Qixun Zeng, Chengyue Sun, Rongfei Jia, Binqiang Zhao, et al. 3d-front: 3d furnished rooms with layouts and semantics. In *ICCV*, 2021. 6, 1
- [9] Zeqi Gu, Yin Cui, Zhaoshuo Li, Fangyin Wei, Yunhao Ge, Jinwei Gu, Ming-Yu Liu, Abe Davis, and Yifan Ding. Artiscene: Language-driven artistic 3d scene generation through image intermediary. In *CVPR*, 2025. 1, 2
- [10] Haonan Han, Rui Yang, Huan Liao, Jiankai Xing, Zunnan Xu, Xiaoming Yu, Junwei Zha, Xiu Li, and Wanhua Li. Reparo: Compositional 3d assets generation with differentiable 3d layout alignment. In *ICCV*, 2025. 2, 6
- [11] Jonathan Ho, Ajay Jain, and Pieter Abbeel. Denoising diffusion probabilistic models. *NIPS*, 2020. 2
- [12] Yicong Hong, Kai Zhang, Jiuxiang Gu, Sai Bi, Yang Zhou, Difan Liu, Feng Liu, Kalyan Sunkavalli, Trung Bui, and Hao Tan. Lrm: Large reconstruction model for single image to 3d. *arXiv*, 2023. 2
- [13] Yujia Hu, Songhua Liu, Xingyi Yang, and Xinchao Wang. Flash sculptor: Modular 3d worlds from objects. *arXiv*, 2025. 1
- [14] Zehuan Huang, Yuan-Chen Guo, Xingqiao An, Yunhan Yang, Yangguang Li, Zi-Xin Zou, Ding Liang, Xihui Liu, Yan-Pei Cao, and Lu Sheng. Midi: Multi-instance diffusion for single image to 3d scene generation. In *CVPR*, 2025. 1, 2
- [15] Nikhil Keetha, Norman Müller, Johannes Schönberger, Lorenzo Porzi, Yuchen Zhang, Tobias Fischer, Arno Knapitsch, Duncan Zauss, Ethan Weber, Nelson Antunes, et al. Mapanything: Universal feed-forward metric 3d reconstruction. *arXiv*, 2025. 4
- [16] Bernhard Kerbl, Georgios Kopanas, Thomas Leimkühler, and George Drettakis. 3d gaussian splatting for real-time radiance field rendering. *TOG*, 2023. 2
- [17] Alexander Kirillov, Eric Mintun, Nikhila Ravi, Hanzi Mao, Chloe Rolland, Laura Gustafson, Tete Xiao, Spencer Whitehead, Alexander C Berg, Wan-Yen Lo, et al. Segment anything. In *ICCV*, 2023. 3, 1
- [18] Kenji Koide. small\_gicp: Efficient and parallel algorithms for point cloud registration. *Journal of Open Source Software*, 2024. 6, 7
- [19] Haoran Li, Haolin Shi, Wenli Zhang, Wenjun Wu, Yong Liao, Lin Wang, Lik-hang Lee, and Peng Yuan Zhou. Dreamscene: 3d gaussian-based text-to-3d scene generation via formation pattern sampling. In *ECCV*, 2024. 1, 6
- [20] Xinhai Li, Huaibin Wang, and Kuo-Kun Tseng. Gaussiandiffusion: 3d gaussian splatting for denoising diffusion probabilistic models with structured noise. *arXiv*, 2023. 2
- [21] Yixun Liang, Xin Yang, Jiantao Lin, Haodong Li, Xiaogang Xu, and Yingcong Chen. Luciddreamer: Towards high-fidelity text-to-3d generation via interval score matching. In *CVPR*, 2024. 2
- [22] Chen-Hsuan Lin, Jun Gao, Luming Tang, Towaki Takikawa, Xiaohui Zeng, Xun Huang, Karsten Kreis, Sanja Fidler, Ming-Yu Liu, and Tsung-Yi Lin. Magic3d: High-resolution text-to-3d content creation. In *CVPR*, 2023. 2
- [23] Haolin Liu, Yujian Zheng, Guanying Chen, Shuguang Cui, and Xiaoguang Han. Towards high-fidelity single-view holistic reconstruction of indoor scenes. In *ECCV*, 2022. 1, 2
- [24] Ruoshi Liu, Rundi Wu, Basile Van Hoorick, Pavel Tokmakov, Sergey Zakharov, and Carl Vondrick. Zero-1-to-3: Zero-shot one image to 3d object. In *ICCV*, 2023. 2
- [25] Shilong Liu, Zhaoyang Zeng, Tianhe Ren, Feng Li, Hao Zhang, Jie Yang, Qing Jiang, Chunyuan Li, Jianwei Yang, Hang Su, et al. Grounding dino: Marrying dino with grounded pre-training for open-set object detection. In *ECCV*, 2024. 1
- [26] Yuan Liu, Cheng Lin, Zijiao Zeng, Xiaoxiao Long, Lingjie Liu, Taku Komura, and Wenping Wang. Syncdreamer: Generating multiview-consistent images from a single-view image. *arXiv*, 2023. 2
- [27] Yanxu Meng, Haoning Wu, Ya Zhang, and Weidi Xie. Scenegenerator: Single-image 3d scene generation in one feedforward pass. *arXiv*, 2025. 1, 2, 6, 7
- [28] Yinyu Nie, Xiaoguang Han, Shihui Guo, Yujian Zheng, Jian Chang, and Jian Jun Zhang. Total3dunderstanding: Joint layout, object pose and mesh reconstruction for indoor scenes from a single image. In *CVPR*, 2020. 1, 2
- [29] Maxime Oquab, Timothée Darcet, Théo Moutakanni, Huy Vo, Marc Szafraniec, Vasil Khalidov, Pierre Fernandez, Daniel Haziza, Francisco Massa, Alaaeldin El-Nouby, et al. Dinov2: Learning robust visual features without supervision. *arXiv*, 2023. 6
- [30] Ben Poole, Ajay Jain, Jonathan T Barron, and Ben Mildenhall. Dreamfusion: Text-to-3d using 2d diffusion. *arXiv*, 2022. 2
- [31] Tianhe Ren, Shilong Liu, Ailing Zeng, Jing Lin, Kunchang Li, He Cao, Jiayu Chen, Xinyu Huang, Yukang Chen, Feng Yan, et al. Grounded sam: Assembling open-world models for diverse visual tasks. *arXiv*, 2024. 1

- [32] Ruoxi Shi, Hansheng Chen, Zhuoyang Zhang, Minghua Liu, Chao Xu, Xinyue Wei, Linghao Chen, Chong Zeng, and Hao Su. Zero123++: a single image to consistent multi-view diffusion base model. *arXiv*, 2023. 2
- [33] Yichun Shi, Peng Wang, Jianglong Ye, Mai Long, Kejie Li, and Xiao Yang. Mvdream: Multi-view diffusion for 3d generation. *arXiv*, 2023. 2
- [34] Roman Suvorov, Elizaveta Logacheva, Anton Mashikhin, Anastasia Remizova, Arsenii Ashukha, Aleksei Silvestrov, Naejin Kong, Harshith Goka, Kiwoong Park, and Victor Lempitsky. Resolution-robust large mask inpainting with fourier convolutions. In *WACV*, 2022. 5
- [35] Stanislaw Szymanowicz, Eldar Insafutdinov, Chuanxia Zheng, Dylan Campbell, Joao F Henriques, Christian Rupprecht, and Andrea Vedaldi. Flash3d: Feed-forward generalisable 3d scene reconstruction from a single image. In *3DV*, 2025. 5, 6, 2
- [36] Jiayang Tang, Zhaoxi Chen, Xiaokang Chen, Tengfei Wang, Gang Zeng, and Ziwei Liu. Lgm: Large multi-view gaussian model for high-resolution 3d content creation. In *ECCV*, 2024. 2
- [37] Jianyuan Wang, Minghao Chen, Nikita Karaev, Andrea Vedaldi, Christian Rupprecht, and David Novotny. Vggv: Visual geometry grounded transformer. In *CVPR*, 2025. 2, 4, 6
- [38] Ning-Hsu Albert Wang and Yu-Lun Liu. Depth anywhere: Enhancing 360 monocular depth estimation via perspective distillation and unlabeled data augmentation. *NIPS*, 2024. 5, 6
- [39] Tianhao Wu, Chuanxia Zheng, Frank Guan, Andrea Vedaldi, and Tat-Jen Cham. Amodal3r: Amodal 3d reconstruction from occluded 2d images. *arXiv*, 2025. 4
- [40] Jianfeng Xiang, Zelong Lv, Sicheng Xu, Yu Deng, Ruicheng Wang, Bowen Zhang, Dong Chen, Xin Tong, and Jiaolong Yang. Structured 3d latents for scalable and versatile 3d generation. In *CVPR*, 2025. 2, 3
- [41] Yue Yang, Fan-Yun Sun, Luca Weihs, Eli VanderBilt, Alvaro Herrasti, Winson Han, Jiajun Wu, Nick Haber, Ranjay Krishna, Lingjie Liu, et al. Holodeck: Language guided generation of 3d embodied ai environments. In *CVPR*, 2024. 1, 2
- [42] Kaixin Yao, Longwen Zhang, Xinhao Yan, Yan Zeng, Qixuan Zhang, Lan Xu, Wei Yang, Jiayuan Gu, and Jingyi Yu. Cast: Component-aligned 3d scene reconstruction from an rgb image. *TOG*, 2025. 2
- [43] Taoran Yi, Jiemin Fang, Junjie Wang, Guanjun Wu, Lingxi Xie, Xiaopeng Zhang, Wenyu Liu, Qi Tian, and Xinggang Wang. Gaussiandreamer: Fast generation from text to 3d gaussians by bridging 2d and 3d diffusion models. In *CVPR*, 2024. 2
- [44] Cheng Zhang, Zhaopeng Cui, Cai Chen, Shuaicheng Liu, Bing Zeng, Hujun Bao, and Yinda Zhang. Deeppanocontext: Panoramic 3d scene understanding with holistic scene context graph and relation-based optimization. In *ICCV*, 2021. 1, 2, 6, 7
- [45] Cheng Zhang, Zhaopeng Cui, Yinda Zhang, Bing Zeng, Marc Pollefeys, and Shuaicheng Liu. Holistic 3d scene understanding from a single image with implicit representation. In *CVPR*, 2021. 1, 2
- [46] Longwen Zhang, Ziyu Wang, Qixuan Zhang, Qiwei Qiu, Anqi Pang, Haoran Jiang, Wei Yang, Lan Xu, and Jingyi Yu. Clay: A controllable large-scale generative model for creating high-quality 3d assets. *TOG*, 2024. 2
- [47] Youcai Zhang, Xinyu Huang, Jinyu Ma, Zhaoyang Li, Zhaochuan Luo, Yanchun Xie, Yuzhuo Qin, Tong Luo, Yaqian Li, Shilong Liu, et al. Recognize anything: A strong image tagging model. In *CVPR*, 2024. 1
- [48] Jia Zheng, Junfei Zhang, Jing Li, Rui Tang, Shenghua Gao, and Zihan Zhou. Structured3d: A large photo-realistic dataset for structured 3d modeling. In *ECCV*, 2020. 6, 1
- [49] Junwei Zhou, Xueting Li, Lu Qi, and Ming-Hsuan Yang. Layout-your-3d: Controllable and precise 3d generation with 2d blueprint. *arXiv*, 2024. 1, 2
- [50] Xiaoyu Zhou, Xingjian Ran, Yajiao Xiong, Jinlin He, Zhiwei Lin, Yongtao Wang, Deqing Sun, and Ming-Hsuan Yang. Gala3d: Towards text-to-3d complex scene generation via layout-guided generative gaussian splatting. *arXiv*, 2024. 1, 2, 6

# Pano3DComposer: Feed-Forward Compositional 3D Scene Generation from Single Panoramic Image

## Supplementary Material

### Overview

This supplementary material provides additional details, including dataset descriptions, implementation details, ablation studies, qualitative results, failure cases, and limitations to complement the main paper. We also provide supplementary videos showcasing qualitative results and rendered 3D scenes, which further demonstrate the effectiveness of our method.

### 7. Datasets

Our experiments involve panorama-to-3D scene composition on synthetic benchmarks and real-world panoramas. Below we summarize the synthetic datasets used for training and quantitative evaluation. 3D-FRONT [8] is a professionally designed dataset comprising high-quality textured furniture models arranged in realistic room layouts. Structured3D [48] is a photo-realistic synthetic dataset featuring rendered images under diverse lighting and furniture configurations, accompanied by rich annotations (semantics, albedo, depth, normals, and layout) but does not release object meshes. For real-world in-the-wild panoramas used in qualitative evaluation, we collect images from public online sources and ensure they are only used for non-commercial research visualization.

### 8. More Implementation Details

**Fine-tune of SceneGen.** To adapt SceneGen [27] for equirectangular panoramic (ERP) inputs, we follow its official data preprocessing pipeline and extend it to handle the equirectangular panoramas rendered from the 3D-FRONT dataset. A representative example of the processed panoramic input, including the panorama, instance masks, and object crops, is shown in Fig. 7. Our model is initialized from the official SceneGen pretrained checkpoint. We fine-tune the model using a global batch size of 8 and an initial learning rate of  $1 \times 10^{-5}$  with AdamW optimizer. The model is trained for 7 days on a single NVIDIA RTX 4090 GPU under mixed-precision (BF16) training.

**Inference.** In our experiments, the input equirectangular panoramas are at a resolution of  $512 \times 1024$ . For evaluation on 3D-FRONT and Structured3D, we directly use the ground-truth instance segmentation annotations provided by each dataset, in the same way as SceneGen [27]. For real-world in-the-wild data, we manually obtain instance masks using the 2D foundation model SAM [17]. To develop a fully automated pipeline, one may

Table 4. Ablation of fine-tuning strategies. “-D”, “-D-F”, and “-D-F-G” indicate progressively freezing DINO, frame, and global attention modules.

Method	CD-S ↓	CD-O ↓	F-Score-S ↑	F-Score-O ↑	IoU-B ↑
Full	0.1883	0.1946	0.4992	0.4907	0.3855
-D	0.1236	0.1177	0.5565	0.5550	0.4360
-D-F	<b>0.0787</b>	<b>0.0765</b>	<b>0.6923</b>	<b>0.6926</b>	<b>0.5679</b>
-D-F-G	0.1120	0.1063	0.5788	0.5850	0.4818

integrate open-vocabulary recognition models (e.g., RAM [47], various visual language models (VLMs)) with detection/segmentation models capable of grounding (e.g., GroundingDINO [25], SAM [17], Grounded-SAM [31]) to identify, localize, and segment objects directly on ERP panoramas. In the Object-World Transformation Predictor, we render 4 multi-view images for each object. We uniformly sample four horizontal viewing directions at azimuth angles  $\{0^\circ, 90^\circ, 180^\circ, 270^\circ\}$ , and apply a fixed  $20^\circ$  downward pitch. All renderings use a resolution of  $518 \times 518$ . These rendered views provide appearance-conditioned geometric cues that significantly stabilize the relative pose estimation stage.



Figure 7. Example inputs of SceneGen.

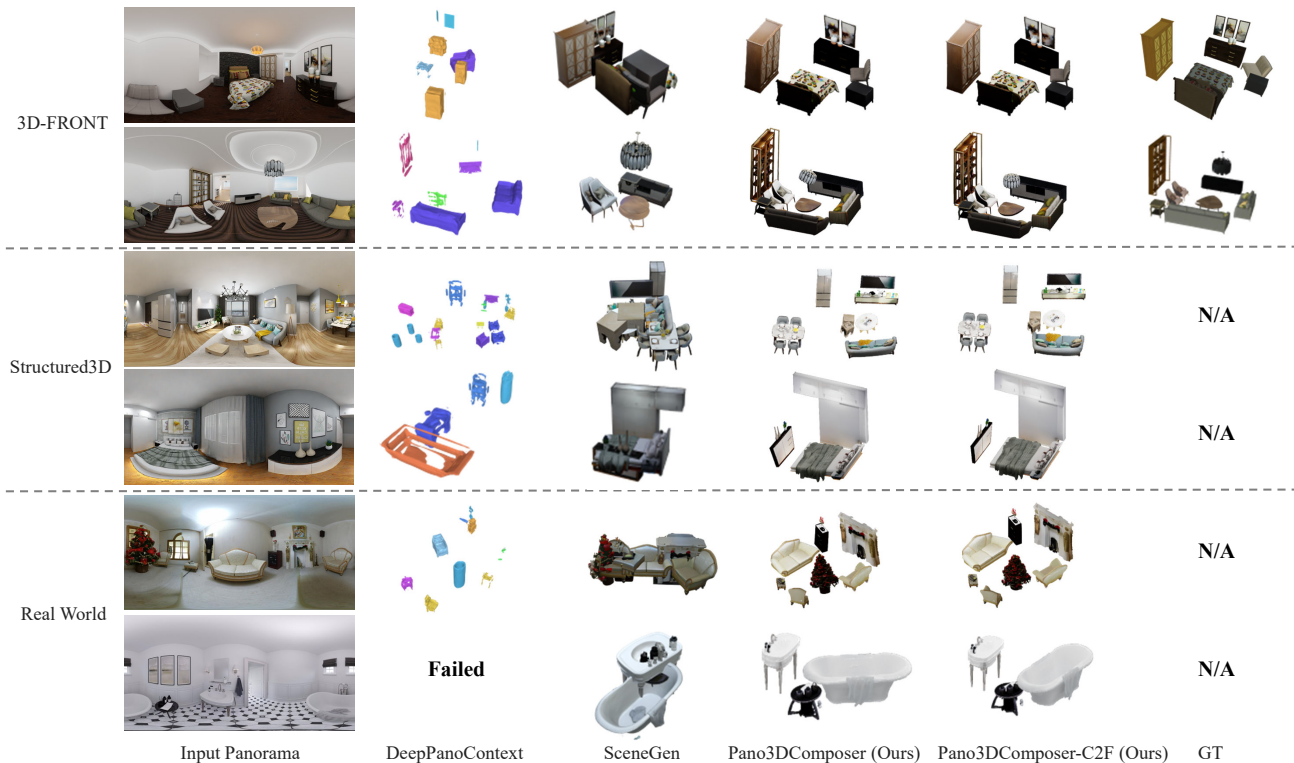


Figure 8. Visualization of panorama-to-3D scene composition results without background.

## 9. More Experiments

### 9.1. Ablation of Trainable VGGT Modules.

We compare different fine-tuning strategies by freezing specific modules of VGGT [37] (Table 4). “Full” denotes full fine-tuning. “-D” freezes the DINO backbone; “-D-F” further freezes the frame attention layers; and “-D-F-G” also freezes the global attention layers. We find that keeping the global attention and camera/scale heads trainable (“-D-F”) yields the largest performance gains across all metrics.

### 9.2. More Visual Comparisons

Fig. 8 shows additional qualitative comparisons between our approach and baselines. To better illustrate the full-room generation capability beyond object synthesis, we provide more rendered videos in the supplementary attachment.

## 10. Failure Cases

When backgrounds exhibit complex geometry, clutter, or heavy occlusions, the inpainting network may fail to recover a clean room structure. This can lead to visible artifacts or incorrect structural completions. In addition, the Flash3D-based [35] monocular reconstruction is affected by

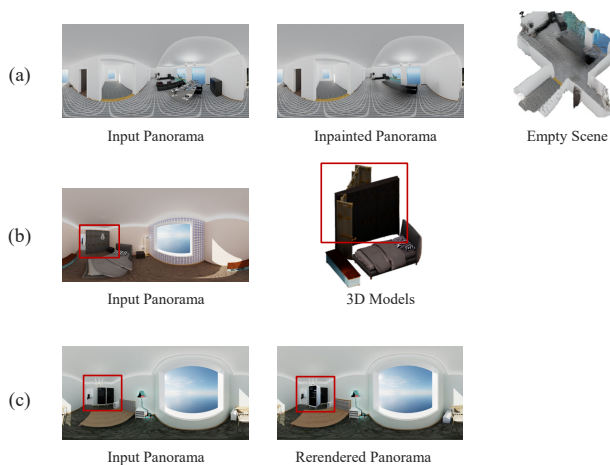


Figure 9. Failure cases. (a) Background inpainting and Flash3D-based monocular reconstruction failures. (b) Object generation failures. (c) Alignment failures.

the quality of depth estimation; inaccurate depth may lead to distorted backgrounds and other artifacts, as illustrated in Fig. 9 (a). Moreover, since the input panorama is constrained to a resolution of  $512 \times 1024$ , the extracted object crops often have relatively low resolution. As a result,

object generation models (e.g., TRELLIS [40]) may occasionally produce suboptimal outputs or even fail to generate plausible results (Fig. 9 (b)).

When the generated 3D object differs drastically from the observed object in the input panorama (in terms of geometry, silhouette, or texture), or when objects in the panorama appear at very low resolution, the alignment network may fail to reliably estimate the relative pose, resulting in misaligned insertions (Fig. 9 (c)).

## 11. Limitations

Our approach primarily targets indoor scenes. Very small items and highly articulated or multi-part objects can still exhibit residual misalignment. Highly glossy or transparent materials pose challenges for appearance modeling and silhouette consistency. Future work includes: (i) integrating physical awareness and multi-instance relation modeling, (ii) improving appearance and geometry prediction for transparent/specular objects, and (iii) scaling training data realism and diversity to further improve generalization.